4.1 Introduction

As demonstrated by past instances, minor changes in the structure and composition of the MOFs result in a dramatic shift in conductivity. This led to the introduction of intrinsically conducting MOF by choosing electroactive ligands or metal ions in specific topologies to avail the charge carrier and conducting pathways. In such MOFs charge transport mainly takes place through space i.e., π- π stacking [1]. Motivated by this characteristic, here UiO-66 has been post-synthetically changed using guest molecules in order to improve and adjust its electrical conductivity. Since this is the case of adding electroactive materials externally to the framework the MOFs obtained through applying this strategy can be termed as extrinsically conducting MOF. This tactic triggers long-range charge delocalization via bonds, spatial arrangements, or the electroactive building blocks' redox behaviour [2].

The electrical conductivity is a property that measures how well electrical charge is transported in a material of interest. It is the product of the charge carrier concentration, n, and the carrier mobility, μ. One of two broad mechanisms—hopping transport or band transport—can adequately explain charge transport in solids from a fundamental standpoint [3]. In the first case, the charge carriers are localised and the charges hop between distinct, nonbonded locations. Such mechanism is usually found in glass, organic semiconductors or disordered materials. Strong site-to-site interactions in the latter case enable the creation of continuous energy bands with delocalized charge carriers. Crystalline and organic materials follow this mechanism. The temperature dependency of these two mechanisms is different. In the hopping transport mechanism, the conductivity elevates thermally and follows an exponential law. In contrast, band transport mechanisms can be activated or deactivated thermally depending on the type of electronic band structure [4].

The earlier works on electrical transport in MOFs were inspired by the works on conducting polymers, coordination polymers, molecular conductors etc. According to Dinca et al. the mechanism behind the conduction in MOFs can be understood by considering three transport phenomena- hoping, through space and through bond [5]. Hoping mechanism basically depends on the charge transfer between donor and acceptor

groups. In this mechanism, charge carriers, such as electrons or holes, are placed at discrete energy levels at specified places and hop between neighbouring positions. The through-space technique complies with the acceptor donor pair requirement as well. Through-space charge transport pathways in MOFs are made possible by non-covalent interactions including π-π stacking between organic components. It is generally known that in organic semiconductors, the charge mobility is directly proportional to the spatial separation that is associated with the magnitude of transfer integral [6]. Analogous to this, linkers that have a great affinity for π–π interactions can produce MOF with high conductivity; in this case, the conduction can be attributed to the organic component [7]. In through bond mechanism charge transfer takes place between metal SBUs and ligand moieties with well-matched energy levels and suitable spatial overlap. To obtain through-bond charge transfer mechanism in MOF one has to choose organic linkers containing N or S functional groups to coordinate with the metal nodes. These linkers will be more electropositive and can facilitate with good orbital overlapping to form a long-range conductive pathway [8].

Motivated by the available literatures on understanding the transport mechanism in MOFs, here, in this work, DC electrical conductivity measurements at room temperature as well as temperature dependent conductivity were studied. This chapter discusses the charge transport phenomena of two electrically conducting MOFs obtained by infiltrating UiO-66 with guest Ag_2O and PEDOT. Distinctly different in terms of structure, yet both the guests chosen are semiconducting in their individual states. After incorporating the guests in UiO-66 how it enhances the conductivity were studied by measuring the current-voltage response of the materials in a two-probe setup with the help of Keithly 2400 source meter in electrodes of ~10 mm width and ~ 100 μm thickness.

4.2 Carrier transport phenomena of S1(MOF) and S2(MOF)

4.2.1 *I-V* characteristics

The room temperature electrical property of Ag_2O, UiO-66, S1(MOF) and S2(MOF) were measured at a linear voltage sweep of -10V to 10 V, with a probe separation 8 mm. In Fig. 4.1, the *I-V* plots of all the samples are presented. As expected, Ag_2O exhibits strong current responsiveness to voltage variations and rectifying properties that highlight its

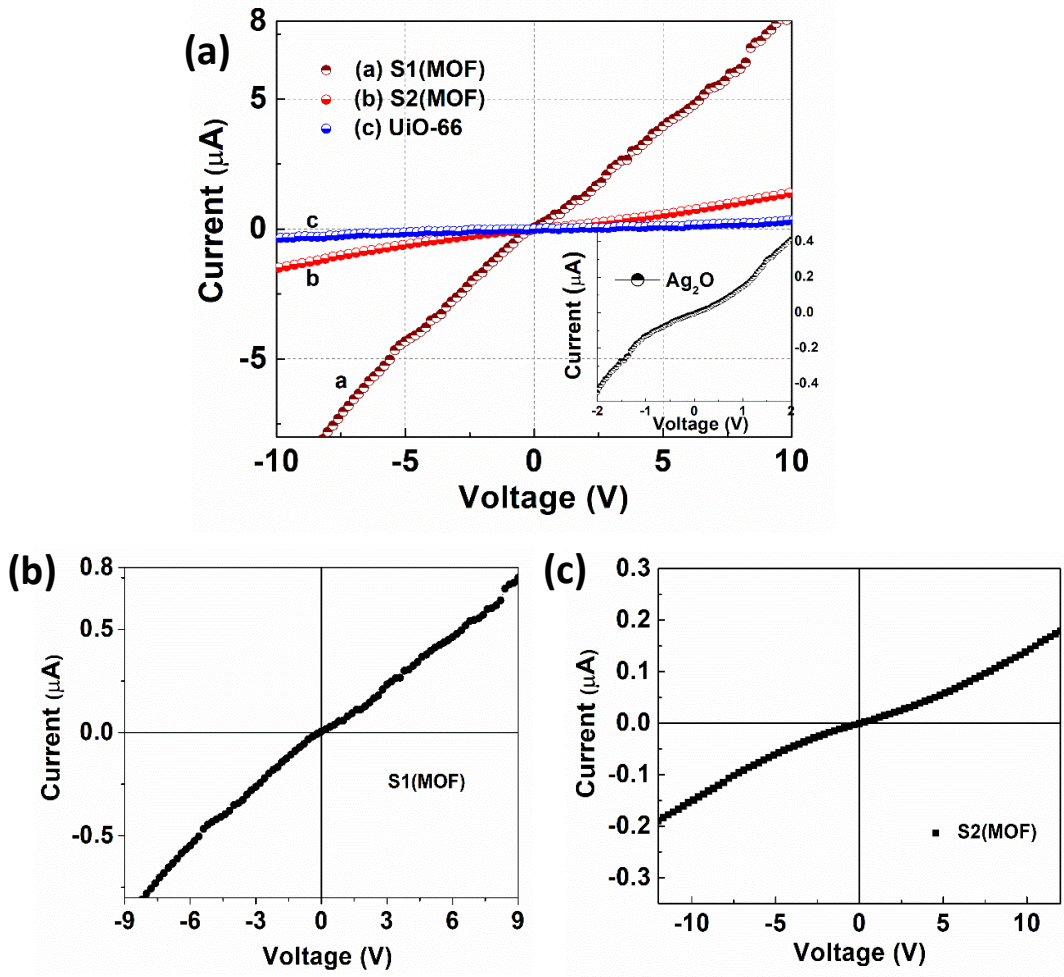

Fig. 4.1. (a) *I-V* plots of UiO-66, S1(MOF), S2(MOF); inset: *I-V* plot of Ag_2O NPs, (b) and (c) *I-V* characteristics of S1(MOF) and S2(MOF) plotted individually.

semiconducting nature. In contrast, UiO-66 shows least current response depicting its insulating nature. However, S1(MOF) and S2(MOF) shows better current response than UiO-66 as a result of Ag_2O NP incorporation in the UiO-66 framework. The *I-V* characteristics of S1 (MOF) exhibit weakly rectifying behaviour, while in S2 (MOF) the non-linear behaviour is apparent, as illustrated in Fig. 4.1. (a) and (b). On analysing the DC conductivity of all the samples using the slope ($G=\Delta I/\Delta V$) of the linear parts of the *I-V* curves, and by employing the popular equation given below.

$$\sigma = \left(\frac{l}{R\mathcal{A}}\right) = \left(G\frac{l}{\mathcal{A}}\right) \text{ S cm}^{-1} \tag{4.1}$$

Here l and $\mathcal{A}$ are probe distance and cross-sectional area; respectively. It was observed that the conductivity of the S1(MOF) and S2(MOF) increased by an order of ten, after

loading Ag_2O NP into the UiO-66 framework. This may be because the interface between the metal NPs and the organic ligands of the MOF can improve charge transport by creating conductive pathways that make it easier for electrons to move within the framework. By improving the electrical coupling between the metal centres and the organic linkers, the metal-organic interface could facilitate profound charge transfer. The values of conductivity of these samples are mentioned in the Table 4.1. The size and distribution of the incorporated metal NPs play a crucial role. Noticeably, the conductivity of S1(MOF) is relatively higher than that of S2(MOF). NPs with smaller sizes may enhance electrical conductivity by providing a more continuous conductive network within the MOF framework. The *I-V* plot of S1(MOF) is predominantly linear with a small rectifying part, it suggests that the material or device exhibits primarily ohmic behaviour with a minor rectifying effect. This indicates that, even at low conductivity levels, the material exhibits the characteristics of an Ohmic resistor in accordance with Ohm's Law, where the current flowing through it is directly proportional to the voltage applied across it.

Table 4.1 DC conductivity of different samples: host and composites.

Sample	**Slope** $G=\Delta I/\Delta V$ **(Ω^{-1})**	**Conductivity** **σ (S cm^{-1})**
UiO-66	2.281 X 10^{-9}	18.25 X 10^{-9}
Ag_2O	1.151 X 10^{-7}	9.2 X 10^{-7}
S1(MOF)	8.819 X 10^{-8}	7.05 X 10^{-7}
S2(MOF)	1.501X 10^{-8}	1.2 X 10^{-7}

The *I–V* characteristics of semiconducting materials were analysed using a few of the most commonly observed transport mechanisms like space charge limited current transport (SCLC), thermally activated current transport, Poole-Frankel conduction, Schottky emission etc [4]. At first the characteristics were examined using the thermionic emission (TE) theory in order to better understand the underlying mechanisms of the charge transport properties of S1(MOF) and S2(MOF).

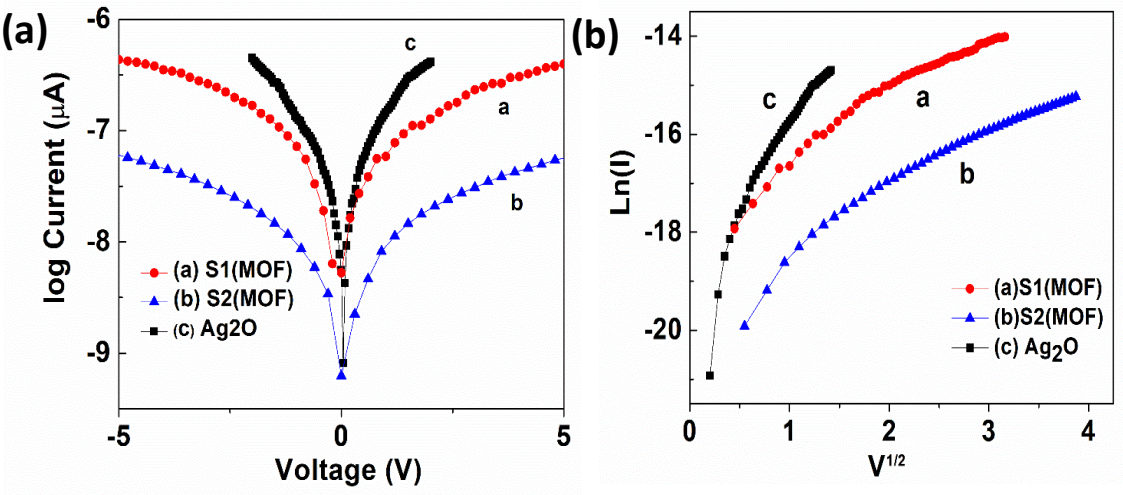

Fig. 4.2. (a) Semi-log plot of current vs. voltage (b) *Log I vs.* $V^{1/2}$ for Ag_2O, S1(MOF) and S2(MOF).

The equation used to fit the plot was-

$$I = I_O\left[exp\left(\frac{qV}{\eta kT}\right) - 1\right] \tag{4.2}$$

where I and I_o are the current at forward bias and reverse saturation current, respectively, q is the electronic charge, η is the ideality factor, k is the Boltzmann factor, T is the absolute temperature [9]. The semi-log plot of I vs. V is not a straight line which is quite evidence for the presence of combination of conduction mechanism like tunnelling, trap charge assisted current, along with thermionic emission (Fig. 4.2). The 'Y' shape of the logarithmic plot depicts the linearly increasing current at the lower bias region while non-linearity at higher bias. According to the previous studies by various researchers at lower bias the current is due to the charge transmission in the foot part of the electronic density rather than the resonance centre [3]. On the other hand, the current will increase more quickly in a nonlinear manner as bias rises and the electrode's electronic level approached to resonate. According to Xianneng Song and colleagues, this kind of logarithmic plot relates to the tunnelling transport mechanism [3]. This analysis can be verified by plotting the current voltage data according to the Richardson's-Schottky thermionic emission model, Flower Nordheim model and Poole-Frankel model which will reveal about the governing mechanism of conduction [10]. However, the plot of Ln (I) vs. $V^{1/2}$ is not a linear one which indicates the absence of thermionic emission (Fig. 4.2 (b)).

Moreover, there is no negative slope in the lower bias of the plot $Ln(I/V^2)$ vs. V^{-1} suggesting the lack of field emission (Fig. 4.3 (a)). The information about the conduction mechanism can also be highlighted by the *I-V* characteristics plotted on a double logarithmic scale. If the slope of double logarithmic plot is ~1, it will follow the Ohm's law where current depends on the applied voltage and if the slope is ~2 the current will depend on a quadratic dependence on voltage and associated with space charge limited current conduction mechanism (SCLC). The SCLC arises when charge carrier movement is restricted by the presence of space charge within the material, particularly at higher electric fields or interfaces. Here in our case the slopes of Ag_2O and S1(MOF) are larger than unity but smaller than 2, which implies that the carriers may follow both SCLC and Ohmic conduction mechanisms. In this combined scenario, lower voltages may primarily exhibit Ohmic behaviour, while higher voltages experience the dominance of SCLC due to the accumulation of charge carriers. The specific value of slope ~ 1.11 indicates a transitional region where both mechanisms contribute significantly to charge transport.

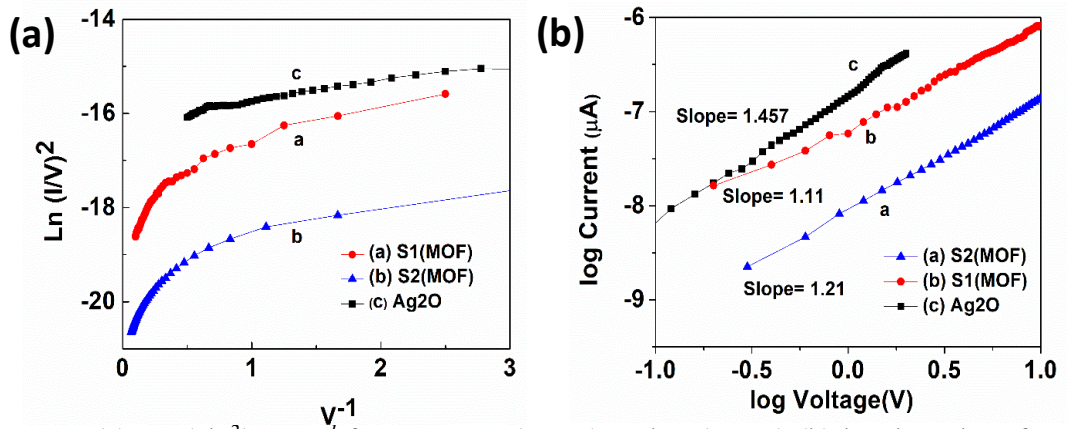

Fig. 4.3. (a) *Ln* (I/V^2) *vs.* V^{-1} for Ag_2O, S1(MOF) and S2(MOF) (b) log-log plot of current and voltage for Ag_2O, S1(MOF) and S2(MOF) systems.

The slope of S2(MOF) is 1.21 in log-log plot. Specifically, slope greater than 1 in a log-log plot indicates a non-linear power-law relationship. This could also be linked to space-charge-limited current (SCLC) or trap-assisted conduction mechanisms. The SCLC mechanism is observed in materials with low carrier concentration or low mobility. When voltage is increased the charge carriers are injected into the semiconducting material which creates an imbalance in the charge distribution and a localized region with accumulated

charges gets formed. This space-charge region creates a depletion layer which limits the flow of current eventually [11]

Repeatability of the data of S1(MOF) and S2(MOF) was checked in five electrodes of similar size under same experimental condition (Fig. 4.4). The plots depict both the material show similar *I-V* characteristics of S1(MOF) and S2(MOF) tested on 5-different electrodes. The standard deviation of five set of data of S1(MOF) and S2(MOF) are found to be ± 1 and ±1.98 which says that the results obtained are consistent throughout the samples.

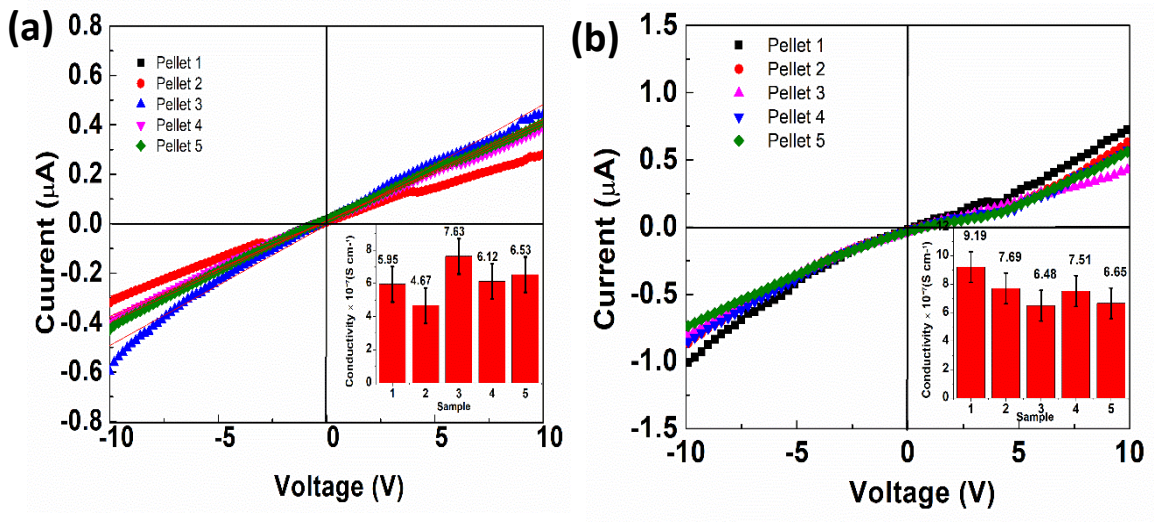

Fig. 4.4. Repeatability test of *I-V* characteristics of (a) S1(MOF) and (b) S2(MOF) on five different electrodes.

4.2.2 Temperature dependent conductivity studies

The temperature dependent conductivity has been measured at a temperature range of 278-338 K. The variation in conductivity with temperature for S1(MOF) and S2(MOF) is presented in Fig. 4.5 (a) and (b). The trend of decreasing conductivity with increasing temperature for both the MOFs is essentially indifferent. When the temperature is increased up to 290 K, a significant drop in conductivity can be observed, further increase in the temperature caused only a minimal change conductivity. Initially, with a moderate increase in temperature, the dominant effect may be the increase in thermal energy, which promotes greater thermal excitation of charge carriers. This increased thermal excitation leads to more frequent carrier scattering events and reduces carrier mobility, thereby

lowering conductivity. This behaviour is typical in many materials, where conductivity decreases with increasing temperature due to increased scattering of charge carriers by lattice vibrations (phonons) or impurities. Beyond a certain temperature threshold, the decrease in carrier mobility due to increased scattering may become negligible or may be offset by other factors like changes in the electronic properties, etc. This could be the reason behind the saturation of conductivity beyond 290 K.

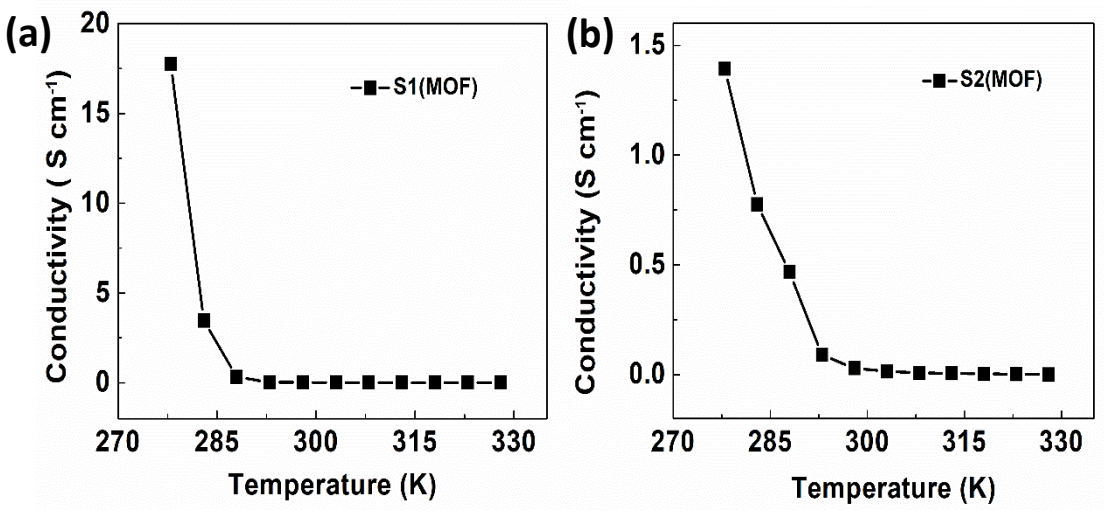

Fig. 4.5. Temperature dependent conductivity of (a) S1(MOF) and (b) S2(MOF) systems.

4.3 Carrier transport phenomena and temperature dependency of PEDOT@UiO-66

4.3.1 *I-V* characteristics

Electrical measurements performed on UiO-66 and PEDOT@UiO-66 MOF composites are presented in terms of the nature of their current profiles when bias voltage was altered in the range of -5 to 5 V (Fig. 4.6). Earlier it was proposed that when oxidising agent/reducing agent is added to the polymer, formation of charge carriers namely, polaron, bipolaron and solitons takes place depending on the structure of the polymer. Accordingly, conductivity is governed by the movement of these charge carriers along the polymer chains [12]. In the conducting polymer (CP), conductivity is the outcome of two processes – either hopping, or tunnelling of localized charge carriers. Hopping conductivity depends on the interchain and intrachain hopping over the conjugation length of the polymer [13]. The DC conductivity of all the samples were obtained by measuring

the slope ($G=\Delta I/\Delta V$) of the linear parts of the *I-V* curves, and by employing the equation 4.1. Know that the UiO-66 MOF is a microporous insulating system in which the carrier transport is rather weak with negligible magnitude of current [14] and the order of conductivity is typically, 10^{-9} S cm^{-1}. The *I-V* curve for PEDOT gave a linear increase in current with increasing voltage (up to 4 V) under both forward and reverse biasing conditions, depicting its Ohmic nature. Upon PEDOT polymerization inside the pores of MOF, the conductivity gets a remarkable enhancement from (2.221± 0.001) × 10^{-3} Scm^{-1} to (3.0± 0.004) ×10^{-2} S cm^{-1}. As predicted earlier through the Raman data, the change in resonating structure of PEDOT from benzoid-to-quinoid conformation could offer a greater number of delocalized electrons and yielding an augmented conductivity. Unlike charge transport concept in inorganic semiconductors, the CPs rely on delocalization and hopping of carriers due to the lack of long-range ordering and periodic lattice structure [15]. The transport in CP occurs taking advantage of disordered chains, kinks and twists as possessed by the backbone of the polymer [16]. As for CPs, it is possible to have inhomogeneous disordered structure with metallic sites separated by some insulating regions [17]. One can study the conduction mechanism and transport phenomenon of such organic semiconductors and its composites using available models for metals, semiconductor, and/or insulators.

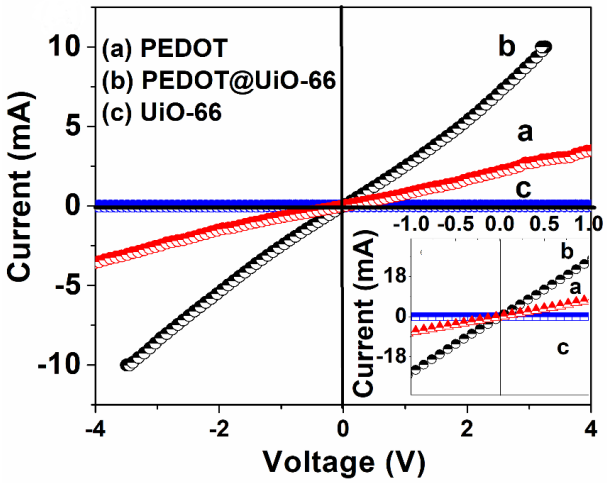

Fig. 4.6. *I-V* curves of PEDOT, PEDOT@UiO-66, and UiO-66 with inset highlighting linear part of the *I-V* curves for a smaller voltage range, from -1 V to 1 V.

The linear or non-linear nature of logarithmic plot of current and voltage provides information about the nature of charge transport. The semi log plots of the *I-V* for PEDOT and PEDOT@UiO-66 MOF at room temperature can be found in Fig.4.7. For both forward and reverse biasing cases, the samples characterize a linear dependency of current on potential at lower bias but at higher bias there is deviation from the linearity aspect and depicting thermionic emission of the carriers in place (Fig. 4.7). The materials seem to follow Richardson-Schottky thermionic emission model where tunnelling through the barrier was discarded and the lowering of barrier caused by the applied field is taken into consideration. According to the model, the current is related to the applied field as follows-

$$I = aT^2 exp[\varphi - (\beta V^{1/2}) / kT] \quad (4.3)$$

where β is related to the dielectric constant of the material, while a is the material dependent constant. The plot of log *I* vs. $V^{1/2}$ would invariably give a straight-line trend [18]. The plots for PEDOT and PEDOT@UiO-66 MOFs are shown in the left inset of Fig. 4.7 in which the line fit characterizes the current transport via thermionic emission events. However, any conduction mechanism due to tunnelling of the carriers is discarded owing to the non-feasibility of the Fowler-Nordheim model in the present case (Fig.4.7 right inset).

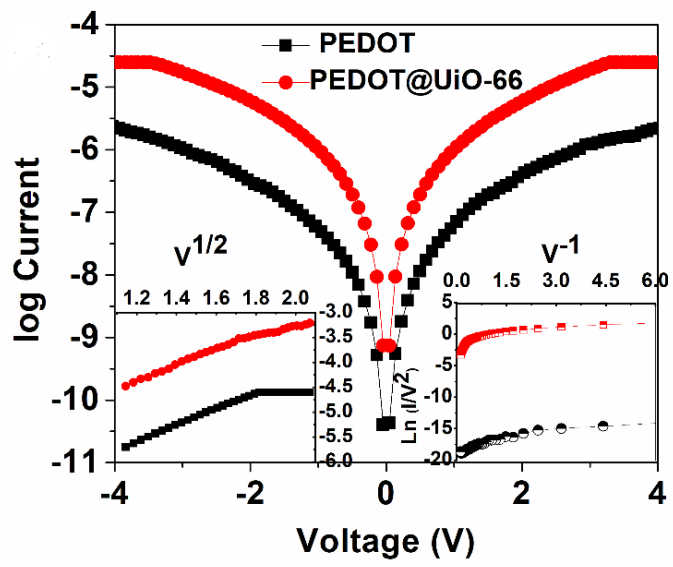

Fig. 4.7. Semi-log plot of *I-V* for PEDOT and PEDOT@UiO-66; Inset- left- *Log I vs.* $V^{1/2}$ and right- *Ln* (I/V^2) *vs.* V^{-1} for PEDOT and PEDOT@UiO-66.

To examine the effect of contact resistance on the *I-V* characteristics of PEDOT@UiO-66 MOFs conductivity of different electrodes of the same sample were compared (Fig. 4.8 (a)). Using transfer length method (TLM), the contact resistance was predicted from the intercept of the linear fit of resistance vs. probe separation curve and typically, ~ (10.8±1.5) Ω for the PEDOT@UiO-66 composite. Also, *I-V* characteristics of different samples of PEDOT@UiO-66 were acquired to check reproducibility and, in this regard, the variation in conductivity found was 0.09 as depicted in the inset of Fig. 4.8 (b) and Table 4.2.

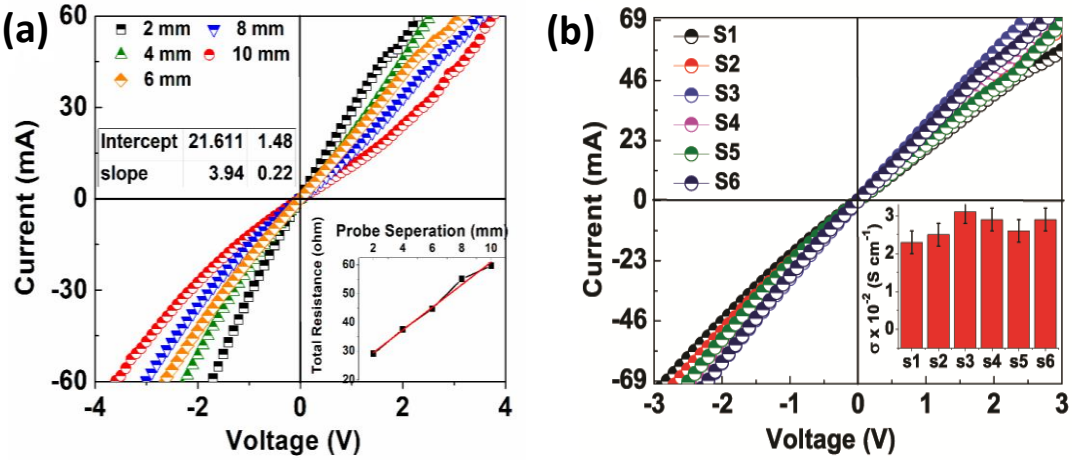

Fig. 4.8. (a) *I-V* curves at different probe separation; Inset- total resistance vs. probe separation, (b) *I-V* curves for different electrodes of PEDOT@UiO-66; Inset- histogram of conductivities for different electrodes.

Table 4.2 DC conductivity of six different electrodes of PEDOT@UiO-66 with deviation.

Sample	**S1**	**S2**	**S3**	**S4**	**S5**	**S6**	**Standard Deviation (±)**	**Variance**
Conductivity x 10^{-2} σ (S cm^{-1})	2.3	2.5	3.1	2.9	2.6	2.9	0.3	0.09

4.3.2 Temperature dependent conductivity studies

Current-Voltage characteristics at room temperature alone cannot give a complete scenario of the charge transport in the system under study and therefore, temperature dependent conductivity responses have been acquired in the temperature range of 273 K to 373 K, as can be found in Fig. 4.9 (a). Apparently, the MOF shows only minimal effect while the PEDOT and PEDOT@UiO66 MOF exhibited thermally activated rise in conductivities with increasing temperature and featuring semiconducting behaviour. In insulating materials, the gap between the conductivity value at room temperature and absolute zero is large because it requires high activation energy for hopping of carriers between sites, the degree of disorder being very high in such materials [19]. The conductivity ratio between higher to lower temperature (303 K), $\sigma_r = \sigma_{373}/\sigma_{303}$ of PEDOT@UiO-66 MOF is less than PEDOT (2.3 and 5 respectively). Unquestionably, the composite has a better semiconducting response than PEDOT only system taking advantage of ample number of π conjugated electrons along the chain backbone which could be delocalized with great ease. Nevertheless, the PEDOT and PEDOT@UiO-66 MOF showed minimal variation in the conductivity features at room and low temperatures due to inherent delocalized states. This delocalization of electronic states takes place when the compact coil conformation of PEDOT changes to elongated conformation. As the conductivity ratio of PEDOT is more one can assume it's degree of disorder to be more than PEDOT@UiO-66 which matches well with the enhanced features of the composite. In CPs the conductivity is due to hopping of charge carriers from one defect site to another within the chain (intra-chain), or from one to the adjacent chain (inter-chain). For short conjugation length, the transport is governed by interchain hopping in both the orthogonal and parallel direction to the chain axis while for long conjugation length conductivity along the chain axis is governed by intrachain carrier transport and in the orthogonal direction conductivities are limited by interchain hopping [20]. In some earlier studies the increase in resistivities was assumed to be the consequence of increasing conjugation length for organic molecular wire. Know that conjugation length largely depends on several factors, like processing route, monomer concentration, doping process etc [21]. An increase in conductivity in the present case may have linkage with the reduction of conjugation length of the chains as PEDOT was polymerized within the restricted space of the micropores provided with enough

monomers. The octahedral pores of UiO-66 can allow only limited number of monomers resulting in PEDOT chains with low conjugation length.

The reduced activation energy plot may reveal more about the temperature dependent conductivity aspect of the samples under study. The hopping transport mechanism of delocalized electrons on account of the variation in conductivity with temperature can be exploited through the relation given below [22] -

$$\sigma(T) = \sigma_o exp\left(-\frac{T_o}{T}\right)^n, \tag{4.4}$$

where σ_o is the limiting value of the conductivity at infinite temperature, T_o is the characteristic temperature and n is the parameter that depends upon conduction mechanism. n is related to the dimensionality of hopping (ζ) by the relation $1/(1+\zeta)$ [22]. Essentially, this parameter is the slope of *log-log* plot of the W vs. T where,

$$W = \frac{dln(\sigma)}{dln(T)} \tag{4.5}$$

Assuming the hopping in PEDOT and PEDOT/UiO-66 to be one dimensional, the semi-log plot, for instance, $ln\ \sigma$ vs. $T^{-1/2}$ can be the one presented in Fig.4.9(b).

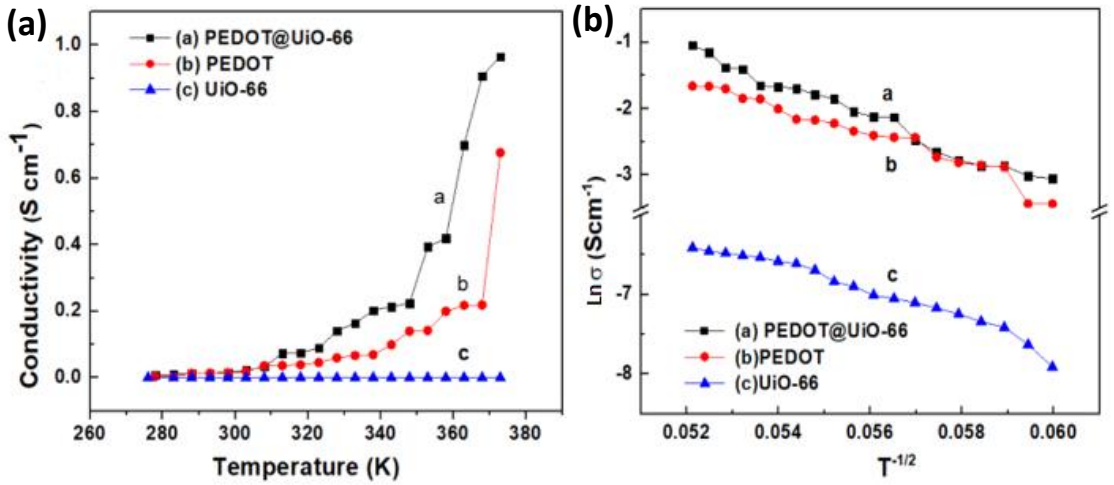

Fig. 4.9. (a) Conductivity vs. temperature for PEDOT@UiO-66, PEDOT and UiO-66 (b) log σ vs. $T^{-1/2}$ plot for the same systems.

We obtained almost linear plots for PEDOT and PEDOT@UiO-66 which can be fitted to Eqn. 5 with n=1/2.This implies that the conductivity mechanism of the composite, to a great extent, follows the Mott's variable hopping (MHV) model like the undoped PEDOT [23]. However, the plot for UiO-66 MOF being insulating in nature has some deviation from the linearity and suggests that MHV model is not fit for explaining the conductivity mechanism of the material.

4.4 Conclusion

The charge transport characteristics of two electrically conducting UiO-66, which were obtained by loading Ag_2O and PEDOT guest molecules into the framework, have been discussed in this chapter. The *I-V* plots of rectifying characters resembling Ag_2O plot with distinct slopes are displayed by both S1(MOF) and S2(MOF) electrodes. The conductivity of UiO-66 increased by 10-fold on introducing the guest into the framework. However, the conductivity of S1(MOF) is more in terms of S2(MOF) may be due to the distribution of NPs over the framework structure. The transport properties have been analysed with the help of various established models. According to which S1(MOF) follows a combined mechanism of Ohmic conduction and SCLC conduction whereas in S2(MOF) SCLC or trap-charge assisted conduction mechanism is seen to be dominant. The temperature-dependent conductivity studies revealed a trend of decreasing conductivity with temperature up to a certain threshold, beyond which the conductivity remained saturated even with further increases in temperature. Such behaviours are generally seen in Ohmic resistors. In summary, the introduction of guest NPs into the structure has created a conduction pathway within the system that potentially expands the material's uses in electronic and electrochemical applications.

The electrical transport properties of PEDOT@UiO-66 has also been discussed. The enhancement in current response was reflected in the current- voltage characteristics of the PEDOT@UiO-66 as compared to UiO-66 and PEDOT. The mechanism behind carrier conduction in this system was assumed to be the thermionic emission. Noticeably, the room temperature conductivity shoots up by nearly ten-fold i.e., from 10^{-3} for PEDOT to 10^{-2} S cm^{-1} for the PEDOT@UiO-66 and 10 million-fold from UiO-66. This result agrees with the possibility of altering conformation leading to a change in the structural

unit, conjugation length of chains, and an increase in hopping probability eventually. The temperature dependence of conductivity profiles of PEDOT and PEDOT confined MOF characterize semiconducting features in the material following the MVH rule across the CP chains. The PEDOT@UiO-66 nanocomposite with an order improvement in conductivity offers a new type of microporous, semiconducting material. More investigation in this direction is required to reveal insights on hopping transport in confined spaces and its applicability to develop hybrid materials with multifunctionalities applicable for energy storage, catalysis and specific sensing purposes etc.

References

[1] Meng, H. *et al.* Conductive Metal–Organic Frameworks: Design, Synthesis, and Applications. *Small Methods*. 4: 2000396, 2020.

[2] Dhara, B. *et al.* Increase in Electrical Conductivity of MOF to Billion-Fold upon Filling the Nanochannels with Conducting Polymer. *Journal of Physical Chemistry Letters*. **7**: 2945–2950, 2016.

[3] Song, X., Han, B., Yu, X. & Hu, W. The analysis of charge transport mechanism in molecular junctions based on current-voltage characteristics. *Chem Phys*. **528**: 110514, 2020.

[4] Rafiq, M. A. Carrier transport mechanisms in semiconductor nanostructures and devices. *Journal of Semiconductors*. **39**: 061002, 2018.

[5] Xie, L. S., Skorupskii, G. & Dincă, M. Electrically Conductive Metal-Organic Frameworks. *Chemical Reviews*. **120**: 8536–8580, 2020.

[6] Coropceanu, V. *et al.* Charge Transport in Organic Semiconductors. *Chem Rev*. **107**: 926–952, 2007.

[7] Guo, L. *et al.* Conductive metal-organic frameworks: Recent advances in electrochemical energy-related applications and perspectives. *Carbon Energy*. **2**: 203–222, 2020.

[8] Han, S. *et al.* Tunneling Electrical Connection to the Interior of Metal-Organic Frameworks. *J Am Chem Soc*. **137**: 8169–8175, 2015.

[9] Sarmah, H. J. & Mohanta, D. Emergence of Raman active D- band and unusually suppressed conductivity mediated by nanoscale defects in pencil-lead graphitic systems under 80 keV Xe+ ion irradiation. *Nucl Instrum Methods Phys Res B*. **463**: 1–6, 2020.

[10] Pandey, S. *et al.* Transition from direct to Fowler–Nordheim tunneling in chemically reduced graphene oxide film. *Nanoscale*. **6**: 3410–3417, 2014.

[11] Rafiq, M. A. Carrier transport mechanisms in semiconductor nanostructures and devices. *Journal of Semiconductors*. **39**: 061002, 2018.

[12] Bredas, J. L. & Street, G. B. Polarons, bipolarons, and solitons in conducting polymers. *Acc Chem Res*. **18**: 309–315, 1985.

[13] Pasveer, W. F. *et al.* Unified Description of Charge-Carrier Mobilities in Disordered Semiconducting Polymers. *Phys Rev Lett*. **94**: 206601, 2005.

[14] Somjit, V. *et al.* Processable UiO-66 Metal–Organic Framework Fluid Gel and Electrical Conductivity of Its Nanofilm with Sub-100 nm Thickness. *ACS Appl Mater Interfaces*. **13**: 30844–30852, 2021.

[15] Das, T. K. & Prusty, S. Review on Conducting Polymers and Their Applications. *Polym Plast Technol Eng*. **51**: 1487–1500, 2012.

[16] Nath, C. & Kumar, A. Doping level dependent space charge limited conduction in polyaniline nanoparticles. *J Appl Phys*. **112**: 093704, 2012.

[17] Kaiser, A. B. Electronic transport properties of conducting polymers and carbon nanotubes. *Reports on Progress in Physics*. **64**: 1–49, 2001.

[18] Roslan, N. A., Supangat, A. & Sagadevan, S. Investigation of Charge Transport Properties in VTP: PC71BM Organic Schottky Diode. *Electronics (Switzerland)*. **11**: 3777, 2022.

[19] Mohan, A., Anil, A. G., Ramamurthy, P. C. & Menon, R. Charge transport in cross-linked PEDOT: PSS near metal–insulator transition. *J Appl Phys*. **131**: 155101, 2022.

[20] Baughman, R. H. & Shacklette, L. W. Conjugation length dependent transport in conducting polymers from a resistor network model. *J Chem Phys*. **90**: 7492–7504, 1989.

[21] Bakhshi, A. K. Electrically conducting polymers: from fundamental to applied research. *Bulletin of Materials Science*. **18**: 469–495, 1995.

[22] SARMAH, S. & KUMAR, A. Electrical and optical studies in polyaniline nanofibre–SnO2 nanocomposites. *Bulletin of Materials Science*. **36**: 31–36, 2013.

[23] Criado-Gonzalez, M., Dominguez-Alfaro, A., Lopez-Larrea, N., Alegret, N. & Mecerreyes, D. Additive Manufacturing of Conducting Polymers: Recent Advances, Challenges, and Opportunities. *ACS Appl Polym Mater*. **3**: 2865–2883, 2021.